The Astronomical Journal, 137:4322–4329, 2009 May doi:10.1088/0004-6256/137/5/4322
© 2009. The American Astronomical Society. All rights reserved. Printed in the U.S.A.

THE ORBITS OF THE NEPTUNIAN SATELLITES AND THE ORIENTATION OF THE POLE OF NEPTUNE

R. A. Jacobson
Jet Propulsion Laboratory, California Institute of Technology, 4800 Oak Grove Drive, Pasadena, CA 91109-8099, USA; robert.jacobson@jpl.nasa.gov
Received 2008 December 1; accepted 2009 February 28; published 2009 April 3

ABSTRACT

This paper reports on an update to the orientation of Neptune's pole and to the orbits of the Neptunian satellites, Triton, Nereid, and Proteus. We determined the new pole and orbits in the International Celestial Reference Frame by fitting them to all available observations through the opposition of 2008. The new data in the fit are high-quality modern astrometry and constitute a 19 year extension of the previous data arc. We assess the accuracy of the orbits and compare them with our earlier orbits. We also provide mean elements as a geometrical description for the orbits.

Key words: ephemerides – planets and satellites: individual (Neptune, Nereid, Proteus, Triton)

1. INTRODUCTION

We produced our previous ephemerides for the Neptunian satellites (Triton and Nereid) and our Neptune pole orientation shortly after the *Voyager* Neptune encounter in August of 1989 (Jacobson 1990; Jacobson et al. 1991). That work was done in the FK4/B1950 reference system, the system adopted for *Voyager* navigation. Since then we have amassed a quantity of high-quality Earth-based observations of the satellites. We have also reconstructed the *Voyager* trajectory in the International Celestial Reference Frame (ICRF; Jacobson 2008). This paper reports on an update to the satellite orbits and Neptune pole based on a new fit, in the ICRF, to observations from the time of the discovery of the satellites through the opposition of 2008. We have added Proteus to our satellite system because it was a *Voyager* optical navigation target and played a role in the *Voyager* reconstruction.

2. ORBIT AND POLE MODEL

The model for the satellite orbits is a numerical integration of their equations of motion (Peters 1981) which are formulated in ICRF Cartesian coordinates centered at the Neptunian system barycenter. Gravitational effects include the attraction of an oblate Neptune, the perturbation of Proteus and Nereid from Triton, and the perturbations of all three satellites due to the Sun, Jupiter, Saturn, and Uranus. Because Proteus and Nereid are small and their masses unknown, we assume that they are massless and, as a consequence, do not gravitationally attract Triton or each other. Gravitational effects of the inner planets are taken into account by augmenting the solar mass with their masses. Neglecting the inner planets simplifies and speeds the integration, and over the 200 year period from 1900 to 2100, introduces errors of at most 3 m for Triton, 7 km for Nereid, and 1 km for Proteus. Such errors are unobservable in our current data. Jet Propulsion Laboratory (JPL) planetary ephemeris DE421 provides the positions of the Sun and planets (Folkner et al. 2008). The use of numerical integration fundamentally changes the representation of Proteus's motion; prior orbits were modeled as precessing ellipses (Owen et al. 1991; Jacobson & Owen 2004).

When computing the force due to Neptune's oblateness, we retain only the second and fourth zonal harmonics. We represent the pole of Neptune by a vector which precesses about the angular momentum of the Neptunian system. This polar motion is driven by the torque due to the gravitational attraction of Triton on the planet's equatorial bulge.

Both Jacobson (1990) and Jacobson et al. (1991) modeled the pole directly as a vector, $\hat{\boldsymbol{h}}$, precessing about an axis, $\hat{\boldsymbol{k}}$, (the direction vector of the system angular momentum), i.e.,

$$\hat{\boldsymbol{h}} = \cos(\dot{\Omega}\,T)\hat{\boldsymbol{h}}_{\boldsymbol{0}} + (\hat{\boldsymbol{h}}_{\boldsymbol{0}}\cdot\hat{\boldsymbol{k}})[1-\cos(\dot{\Omega}\,T)]\hat{\boldsymbol{k}} + \sin(\dot{\Omega}\,T)\times(\hat{\boldsymbol{h}}_{\boldsymbol{0}}\times\hat{\boldsymbol{k}}) \tag{1}$$

with $\hat{\boldsymbol{h}}_{\boldsymbol{0}}$ being the pole at epoch, $\dot{\Omega}$ the precession rate, and T the time from epoch. The unit vector normal to Triton's orbit, $\hat{\boldsymbol{w}}$, also precesses about the system angular momentum with the same rate as the Neptune pole. Its direction was specified by

$$\hat{\boldsymbol{w}} = \frac{(\boldsymbol{r}_1\times\dot{\boldsymbol{r}}_1)}{|\boldsymbol{r}_1\times\dot{\boldsymbol{r}}_1|} = \hat{\boldsymbol{k}}\cos\,I + [\hat{\boldsymbol{p}}\sin(\Omega_0+\dot{\Omega}\,T) - \hat{\boldsymbol{q}}\cos(\Omega_0+\dot{\Omega}\,T)]\sin\,I, \tag{2}$$

where $\boldsymbol{r}_1$, $\dot{\boldsymbol{r}}_1$ are Triton's barycentric position and velocity, I is the angle between Triton's orbit normal and the system angular momentum, and Ω_0 is the epoch value of ascending node of Triton's orbit on the plane normal to $\hat{\boldsymbol{k}}$. The coordinate axes were

$$\hat{\boldsymbol{p}} = (\hat{\boldsymbol{e}}_{\boldsymbol{3}}\times\hat{\boldsymbol{k}})\sec\delta_r \qquad \hat{\boldsymbol{q}} = \hat{\boldsymbol{k}}\times\hat{\boldsymbol{p}}, \tag{3}$$

where $\hat{\boldsymbol{e}}_{\boldsymbol{3}}$ is the unit vector (0, 0, 1) and δ_r is the declination of $\hat{\boldsymbol{k}}$. The components of the Neptune and Triton angular momentum normal to the system angular momentum were related by

$$\left[1-\left(1-\frac{J_2}{\gamma}\right)\left(\frac{\dot{\Omega}}{\dot{W}}\right)\cos\epsilon\right]\sin\epsilon = \frac{\mu_1\mu_s^2}{(\mu_s-\mu_1)^3}\frac{\sin\,I\;|\boldsymbol{r}_1\times\dot{\boldsymbol{r}}_1|}{\gamma R^2\dot{W}}, \tag{4}$$

where ϵ is the angle between $\hat{\boldsymbol{h}}$ and $\hat{\boldsymbol{k}}$, J_2 is second zonal harmonic of Neptune's gravitational potential, γ is Neptune's axial moment of inertia factor, $\dot{W}$ is Neptune's spin rate, μ_s is the GM of the Neptunian system, μ_1 is the GM of Triton, and R is the equatorial radius of Neptune. Note: GM is the product of the Newtonian constant of gravitation G and the mass M. The pole was determined as part of the orbit fitting process by estimating the pole direction at epoch, the precession axis, the

precession rate, and the Triton orbital inclination and ascending node at epoch. To constraint the solution, the expressions

$$\hat{\boldsymbol{h}} \cdot \hat{\boldsymbol{k}} = \cos\epsilon \tag{5}$$

$$\hat{\boldsymbol{w}} \cdot \hat{\boldsymbol{k}} = \cos\, I \tag{6}$$

$$\hat{\boldsymbol{w}} \cdot \hat{\boldsymbol{p}} = \sin\, I \sin\left(\Omega_0 + \dot{\Omega}\, T\right) \tag{7}$$

and Equation (4) were required to hold in a least-squares sense over the data processing time span.

For the current analysis we adopt a different approach for representing the pole. The pole's orientation angles can be expressed in the form

$$\begin{aligned} \tan\left(\alpha - \alpha_r\right) &= \frac{\tan\epsilon \sec\delta_r \sin\Omega}{1 + \tan\epsilon \tan\delta_r \cos\Omega} \\ \sin\delta &= \sin\delta_r \cos\epsilon - \cos\delta_r \sin\epsilon \cos\Omega \end{aligned} \tag{8}$$

where α and δ are the pole right ascension and declination, α_r and δ_r are the right ascension and declination of the system angular momentum, and $\Omega = \Omega_0 + \dot{\Omega}\, T$. Because ϵ is a small angle the above expressions can be expanded into series. Retaining terms to order ϵ^2, the series are

$$\alpha = \alpha_r + \epsilon \sec\delta_r \sin\Omega - \frac{1}{2}\epsilon^2 \sec\delta_r \tan\delta_r \sin\, 2\Omega \tag{9}$$

$$\delta = \delta_r - \epsilon \cos\Omega - \frac{1}{4}\epsilon^2 \tan\delta_r \left(1 - \cos\, 2\Omega\right). \tag{10}$$

We compute the pole from the series rather than the vectorial model (1) or expressions (8) because series are the standard IAU/IAG representation for the rotational elements of solar system bodies (Seidelmann et al. 2007). Moreover, the series are needed for compatibility with the JPL navigation software which uses the IAU/IAG standard for orienting all solar system planets and satellites except for the Earth, Moon, and Mars. (Note: the series model for planets was not adopted for JPL navigation until after the end of the Galileo extended mission in 2002, i.e., it was not in use at the time of the *Voyager* mission).

In our data fit we estimate α_r, δ_r, ϵ, I, Ω_0, and $\dot{\Omega}$. As before we employ Equations (4) and (6) to constrain the solution, but we have replaced Equation (7) with

$$\hat{\boldsymbol{w}} \cdot \left(\hat{\boldsymbol{p}} \cos\Omega + \hat{\boldsymbol{q}} \sin\Omega\right) = 0 \tag{11}$$

because it is numerically superior; Equation (5) is no longer needed.

3. OBSERVATIONS

We fit the integrated orbits to all of the observations used previously plus those collected since 1989. The observation set contains: Earth-based astrometric observations of all three satellites, *Hubble Space Telescope* (*HST*) observations of Proteus, imaging observations of all three satellites made by the *Voyager* spacecraft, the *Voyager* radiometric tracking used in the trajectory reconstruction, the Triton occultation of the spacecraft observed by the *Voyager* Radio Science Team, and the Triton occultation of the star β Canis Majoris observed with the *Voyager* Ultraviolet Spectrometer.

Proteus was discovered by the *Voyager* Science Team; it was later seen from the Earth (Colas & Buil 1992; Martins et al. 2004; Marchis et al. 2004) and from *HST* (Pascu et al. 1999; Dumas et al. 2002). Jacobson & Owen (2004) report on the previous determination of Proteus's orbit and analyze the Earth-based and *HST* observations.

The Triton astrometry covers the 161 years from 1847 (one year after discovery) through 2008 and includes visual, photographic, and couple device (CCD) observations. Nereid's astrometry, photographic and CCD, covers the 59 years from its discovery in 1949 through 2008. Prior to 1989 the observations of both satellites were either visual or photographic and, except for a small number of Nereid observations, were measures of the satellite's position relative to Neptune. Our previous papers discuss these observations in detail. Post-1989 the astrometry was done with CCDs leading to a significant improvement in measurement accuracy. Those data consist of

1. Triton and Nereid observations from the Laborat'orio Nacional de Astrof'isca in Brazil (1991–2002) (Veiga et al. 1996, 1999; Veiga & Vieira Martins 1996, 1998; Martins et al. 2004),
2. Triton observations from the USNO at Flagstaff (1995–2008) (Stone & Harris 2000; Stone 2000, 2001) and (private communications from R. C. Stone 2002, 2003, 2004, 2005; A. K. B. Monet 2006, 2007; H. Harris 2007, 2008),
3. Triton observations from Table Mountain Observatory (1999–2008) (W. M. Owen 2001, 2003, 2004, 2006, 2007, 2008, private communications),
4. Triton meridian circle observations from Bordeaux Observatory (1999–2005) (Arlot et al. 2008),
5. Triton observations from the Sheshan Station of the Shanghai Astronomical Observatory (1996–2006) (Qiao et al. 2007),
6. Nereid observations from McDonald Observatory (1993–1994) (A. L. Whipple 1995, private communication),
7. Nereid observations from the USNO at Flagstaff (1998) (A. K. B. Monet 1998, private communication),
8. Nereid observations from the Xinglong Station of the Chinese Academy of Sciences National Observatory (2006–2007) (Qiao et al. 2008), and
9. Nereid observations (1990–2008) that were reported by several observers to the Minor Planet Center at the Smithsonian Astrophysical Observatory.

For the most part the post-1989 data are the ICRF right ascension and declination of the satellite. Veiga's data, however, are positions of the satellite relative to Neptune. It is noteworthy that there has been a large increase in the number of Nereid Earth-based observations, from a total of 74 before 1989 to 651 after 1989.

The *Voyager* imaging data are pictures of the satellites against a stellar background which provides the pointing reference for the spacecraft camera. We added seven Triton images and six Nereid images that were omitted in our earlier work. We also replaced the reference star positions, originally in the FK4/B1950 system, with ICRF positions from the UCAC2 star catalog. We should emphasize that the data are the original imaging data and not the reduced astrographic form published in Jacobson (1991).

Doppler tracking and ranging constitute the *Voyager* radiometric data. They provide crucial information on the dynamical

parameters of the Neptunian system, namely, the system and Triton GMs, Neptune's gravity field, and Neptune's pole orientation. See Lewis et al. (1992) and Jacobson (2008) for a complete description of the data.

The occultation data, which are the times of occultation ingress and egress, help fix Triton's position near the time of the spacecraft flyby. Consequently, they aid in the determination of Triton's GM from the spacecraft data. For the stellar occultation we took the star position from the UCAC2 star catalog.

The most accurate data are from the *Voyager* images. They provide position measures with an accuracy ranging from a few 100 km to better than 5 km, depending on the distance between the spacecraft and satellite. The best astrometric data give positions good about 1000 km. The *Voyager* data span less than one year for Triton and only four months and three months for Nereid and Proteus, respectively. Consequently, the satellites' long period motion cannot be determined solely from the *Voyager* data. The overall orbits must be found from the combined short arc of high accuracy spacecraft data and the long arc of lower accuracy Earth-based data.

4. SOLUTION METHOD AND RESULTS

We determined the orbits by adjusting the parameters in our dynamical and observational models to fit the data in a weighted least-squares sense (Tapley et al. 2004). The dynamical parameters are (1) the epoch position and velocity of each satellite, (2) the GMs of the Neptunian system and Triton, (3) the second and fourth zonal harmonics in the Neptune gravitational field, (4) the right ascension and declination of the system angular momentum, (5) the angle between the Neptune pole and the system angular momentum, (6) the angle between Triton's orbit normal and the system angular momentum, and (7) the pole precession angle at epoch and the pole precession rate.

The observational model parameters are

1. Observation biases for the Nereid observations of Van Biesbroeck (1951, 1957) and Van Biesbroeck et al. (1976) to account for systematic errors; as was done previously, separate biases are estimated for each opposition.
2. Observation biases for the Triton observations of Qiao et al. (2007); separate biases are estimated for each night. In his paper R. C. Qiao alluded to the presence of systematic errors in his observations and speculated that they may be due to orbit errors. We detected systematic errors which varied among the nights of the observations. The errors could not be removed with orbit corrections. Moreover, we ascertained that if no allowance were made for the systematic errors, including Qiao's data degraded the fit to the other observations.
3. A refraction correction for the observations from Bordeaux Observatory; the published observations exhibit a systematic error which can easily be removed with a small correction for refraction. We speculate there may have been a problem with the original refraction calibration.
4. The radius of Triton used in the Triton occultation observation constrained to the 1352.6 km value determined from *Voyager* imaging (Davies et al. 1991) by its 2.4 km uncertainty; the constraint on the radius is about a factor of 3 tighter than that imposed in the earlier analysis due to improved knowledge of the radius.
5. The location of star occulted by Triton constrained to its catalog position by the uncertainty quoted in the catalog (15 mas).
6. Camera pointing angles for the *Voyager* imaging observations.

As a part of the processing, we forced the angular momentum balance (Equation (4)) and the expressions defining Triton's inclination (Equation (6)) and the precession angle (Equation (11)) to be satisfied, in a least-squares sense, over a four-century time span from 1800 to 2200 (a bit more than half a precession period).

In keeping with our prior work, the astrometric data are grouped according to data type, observatory, and the observing period during which they were acquired. We take the accuracy of each group to be equal to the rms of the residuals of the group and set the data weights in accordance with that accuracy. For the *Voyager* imaging data we retained the 0.5 pixel accuracy assumption for Triton but changed the accuracy for Nereid to 0.5 pixel, for Proteus to 1.0 pixel, and for the background stars to 0.25 pixel. These new values are about a factor of two better than the overly pessimistic ones assumed earlier. As before, the post-encounter Triton images are systematically deweighted up to 2.0 pixel accuracy because of centerfinding problems introduced by their high phase angles. The weights on the occultation observations matched those of our earlier work, but for the radiometric data we adopted a new weighting technique initially developed for Cassini navigation. The revised Doppler data weights are set by scaling the rms of the residuals for each tracking pass by a specific factor to account for the fact that Doppler noise is not a white-noise process. The range data weights are scaled to effectively compress the range data acquired during each tracking pass into a single measurement for that pass. The scaling suppresses range rate information inferred from the change in range during the pass and allows the Doppler to become the primary measure of range rate. See Jacobson (2008) for further details on the *Voyager* data weights.

Because the fit to the pre-1989 data yields residuals comparable to those from our previous orbits we will not give the statistics for those residuals in this paper. The rms of the residuals for the post-1989 observations appears in Tables 1 and 2; α denotes ICRF right ascension, δ denotes declination, and $\Delta\alpha\cos\delta$,$\Delta\delta$ are positions of the satellite relative to Neptune. For Whipple's data we differenced the simultaneously observed positions of Nereid and Neptune. Table 3 contains the rms for the updated *Voyager* imaging data.

Tables 4 and 5 give the epoch state vectors and the dynamical parameters determined from the fit together with the additional parameters needed for the pole model, namely Neptune's axial moment of inertia factor and spin rate; the vector components and parameters are specified to 16 digits to facilitate future orbit integrations. For comparison purposes, Table 5 includes the parameter values from our previous work (Jacobson et al. 1991). The errors quoted in the table are the formal 1σ statistics (we could find no record of the uncertainties for the previous ϵ, I, or Ω_0). Neptune's spin rate is that of its magnetic field as determined with measurements from *Voyager* (Warwick et al. 1989). This spin is presumed to be the spin of the bulk of Neptune which is a differentially rotating fluid planet. Neptune's moment of inertia is computed from the Radau–Darwin approximation for a fluid planet (Zharkov & Trubitsyn 1978); the approximation relates the moment of inertia to the planet's GM, rotation rate, equatorial radius, and flattening. We

Table 1
Triton Observation Residual Statistics

Source	No.	Type	rms	No.	Type	rms
Veiga et al. (1996)	51	$\Delta\alpha \cos\delta$	0.″080	51	$\Delta\delta$	0.″046
Veiga & Vieira Martins (1996)	422	$\Delta\alpha \cos\delta$	0.″099	422	$\Delta\delta$	0.″138
Veiga & Vieira Martins (1998)	759	$\Delta\alpha \cos\delta$	0.″156	759	$\Delta\delta$	0.″212
Stone & Harris (2000)	402	α	0.″142	402	δ	0.″167
Stone (2000)	114	α	0.″112	114	δ	0.″103
Owen (2001, private communication)	6	α	0.″059	6	δ	0.″018
Stone (2001)	162	α	0.″091	162	δ	0.″113
Stone (2002, private communication)	133	α	0.″098	133	δ	0.″110
Owen (2003, private communication)	50	α	0.″042	50	δ	0.″058
Stone (2003, private communication)	152	α	0.″093	152	δ	0.″108
Martins et al. (2004)	65	α	0.″135	65	δ	0.″119
Owen (2004, private communication)	57	α	0.″063	57	δ	0.″065
Stone (2004, private communication)	145	α	0.″084	145	δ	0.″108
Stone (2005, private communication)	164	α	0.″094	164	δ	0.″124
Monet (2006, private communication)	135	α	0.″115	135	δ	0.″124
Owen (2006, private communication)	4	α	0.″080	4	δ	0.″031
Arlot et al. (2008)	184	α	0.″089	184	δ	0.″119
Monet (2007, private communication)	22	α	0.″077	22	δ	0.″110
Harris (2007, private communication)	81	α	0.″102	81	δ	0.″145
Owen (2007, private communication)	26	α	0.″082	26	δ	0.″087
Qiao et al. (2007)	940	α	0.″039	940	δ	0.″032
Owen (2008, private communication)	30	α	0.″074	30	δ	0.″086
Harris (2008, private communication)	123	α	0.″115	123	δ	0.″149

Table 2
Nereid Observation Residual Statistics

Source	No.	Type	rms	No.	Type	rms
Whipple (1995, private communication)	3	$\Delta\alpha$	0.″520	3	$\Delta\delta$	0.″181
Veiga et al. (1996)	7	$\Delta\alpha \cos\delta$	0.″210	7	$\Delta\delta$	0.″310
Monet (1998, private communication)	4	α	0.″183	4	δ	0.″092
Veiga et al. (1999)	171	$\Delta\alpha \cos\delta$	0.″185	171	$\Delta\delta$	0.″125
Veiga et al. (1999)	56	α	0.″123	56	δ	0.″155
MPC (2000)	9	α	0.″439	9	δ	0.″555
MPC (2001)	6	α	0.″486	6	δ	0.″196
MPC (2002)	6	α	0.″282	6	δ	0.″120
MPC (2003)	1	α	0.″451	1	δ	0.″262
MPC (2004)	30	α	0.″428	30	δ	0.″298
MPC (2005)	39	α	0.″314	39	δ	0.″333
MPC (2006)	104	α	0.″332	104	δ	0.″323
MPC (2007)	76	α	0.″229	76	δ	0.″314
MPC (2008)	27	α	0.″426	27	δ	0.″397
Qiao et al. (2008)	112	α	0.″208	112	δ	0.″188

Table 3
Voyager Imaging Residuals RMS

Object	No.	Sample	Line
Triton	366	0.200	0.170
Nereid	89	0.320	0.244
Proteus	183	0.353	0.262
Stars	1340	0.142	0.133

have adopted the moment of inertia associated with the current Neptune interior model (Hubbard et al. 1995). However, we have scaled it to account for a change from Hubbard's reference radius of 24,764 km to our reference radius of 25,225 km. The value is larger than that we used previously primarily due to an increase in Neptune's flattening from 0.0174 assumed at the time of the *Voyager* encounter (Gerschultz 1989) to Hubbard's post-encounter 0.0182. Our new values for the GMs and harmonics agree with those obtained earlier, however the improved *Voyager* data weighting strategy has reduced their uncertainties. The revised pole model yields an orientation at epoch (1989 August 25) of $\alpha = 299.^{\circ}375$ and $\delta = 42.^{\circ}949$ which matches our previously determined orientation of $\alpha = 299.^{\circ}272$ and $\delta = 42.^{\circ}947$ within the uncertainties. Overall the two pole models exhibit periodic differences with amplitudes of at most $0.^{\circ}16$ in right ascension and $0.^{\circ}09$ in declination.

Table 4
Barycentric State Vectors at 1989 October 31 (TDB)

Satellite	Position (km)	Velocity (km s^{-1})
Triton	−281877.3536356403	1.947557389720039
	−52117.12036252407	2.288229023886188
	208875.6793604145	3.199140819566380
Nereid	4391344.992741283	−0.2010892269240093
	6247989.994965501	0.5283634977506508
	3506876.435467631	0.2598964795227514
Proteus	69308.76609904459	−5.520236069734511
	84473.13614791310	2.007384008752982
	43611.93549123633	4.860915026220256

Notes. The timescale for JPL ephemerides is Temps Dynamique Barycentrique, Barycentric Dynamical Time (TDB) (IAU 2006)

Table 5
Dynamical Parameters

Param.	Jacobson et al. (1991)	Current
GM (km^3 s^{-2})		
System	6836534.9 ± 15.0	6836527.100580397 ± 10.0
Triton	1427.9 ± 3.5	1427.598140725034 ± 1.9
$J_2(\times 10^{-6})$	3410.5 ± 9.0	3408.428530717952 ± 4.5
$J_4(\times 10^{-6})$	−34.7 ± 10.0	−33.398917590066 ± 2.9
α_r (deg)	299.364 ± 0.15	299.4608612607558 ± 0.14
δ_r (deg)	43.449 ± 0.10	43.4048107907141 ± 0.03
ϵ (deg)	0.506	0.4616274249865 ± 0.001
I (deg)	156.834	156.8698869067950 ± 0.01
Ω_0 (deg)	352.433[a]	352.1753923868973 ± 0.11[a]
$\dot{\Omega}$ (deg century^{-1})	52.318 ± 0.25	52.3836218446110 ± 0.26
$\dot{W}$ (deg day^{-1})	536.3128492 ± 1.66[b]	536.3128492 ± 1.66[b]
γ	0.21[c]	0.23 ± 0.01[d]

Notes. Reference radius for the gravitational harmonics: 25,225 km.
[a] Epoch: 1989 August 25.
[b] Not estimated, from Warwick et al. (1989).
[c] Not estimated, from Gerschultz (1989).
[d] Not estimated, from Hubbard et al. (1995).

5. MEAN ORBITAL ELEMENTS

To permit a geometric description of the orbits we computed the mean orbital elements provided in Table 6. The elements for Triton and Nereid are derived by fitting a precessing ellipse to each integrated orbit over the 400 year time span from 1800 January 1 to 2200 January 1; for Proteus the time span is 1950 January 1 to 2050 January 1. The ellipses represent planetocentric orbits for Triton and Proteus, but for the more distant Nereid, the ellipse describes a barycentric orbit. The reference plane for the elements is the local Laplace plane of each satellite (the ellipses precess at constant inclination about the Laplace plane poles). The pole directions for the Laplace planes appear in the table; they are determined as part of the fitting process. As expected, Triton's Laplace plane pole matches the system angular momentum direction in Table 5 within its uncertainties. The orbital longitudes are measured from the intersection of the Laplace plane with the ICRF

Table 6
Mean Elements at 2000 January 1.5 (TDB) Referred to the Local Laplace Planes

Element	Triton	Nereid	Proteus
a(km)	354759.	5513818.	117646.
e	0.00001	0.75074	0.00051
ϖ(deg)	248.5342	256.6874	23.0994
λ(deg)	240.7909	113.3797	274.0371
i(deg)	156.8650	7.0903	0.0749
Ω(deg)	177.6075	335.5701	315.1314
$\dot{\lambda}$(deg day^{-1})	61.2572638	0.9996276	320.7656245
$\dot{\varpi}$(deg yr^{-1})	0.4081	0.0064	28.1362
$\dot{\Omega}$(deg yr^{-1})	0.5237	−0.0381	−28.2873
α^{a}(deg)	299.4560	269.3023	299.4058
δ^{a}(deg)	43.4141	69.1166	42.4317

Note. [a] Laplacian plane right ascension and declination.

reference plane. Note that because Triton's orbit is retrograde, $\varpi = \Omega - \omega$ where ω is the argument of periapsis; for the other two satellites $\varpi = \Omega + \omega$.

6. COMPARISON WITH THE PREVIOUS ORBITS

Figures 1–3 show the differences between our previous satellite orbits (Jacobson et al. 1991; Jacobson & Owen 2004) and the current ones in terms of the radial direction from the planet, the transverse (normal to the radius) direction, and the direction normal to the orbit plane. Slopes in the transverse differences indicate changes in the mean motions of all three satellites. The change in the Triton and Proteus orbits in the normal direction is primarily a consequence of differences in their orbital precession due to the Neptune gravitational harmonics. The Nereid out-of-plane change is simply the result of an inclination change; because Nereid is more distant from the planet its orbit precesses slowly and changes in the precession are not evident in the comparison time period.

The large amplitude periodic signatures in Nereid's radial and transverse directions are directly related to the mean motion differences in this satellite's highly eccentric orbit. The orbit differences may be approximated by

$$\Delta R \approx V_r\,(\Delta n/n)\,t \;\approx\; a(1-e^2)^{-1/2}\,(e\sin f)\,\Delta n\,t \qquad (12)$$

$$\Delta T \approx V_t\,(\Delta n/n)\,t \;\approx\; a(1-e^2)^{-1/2}\,(1+e\cos f)\,\Delta n\,t, \qquad (13)$$

where ΔR is the difference in the radial direction, ΔT is the difference in the transverse direction, V_r is the radial velocity, V_t is the transverse velocity, n is the mean motion, Δn is the difference in the mean motion, a is the orbit semimajor axis, e is the orbit eccentricity, f is the orbit true anomaly, and t is the time from epoch. From Figure 2(b) we see that the amplitude of ΔR is about 6000 km in 2050. Based on that amplitude and Nereid's elements from Table 6, we deduce $\Delta n\,t = 9.6 \times 10^{-4}$ radians in 2050. It follows from Equation (13), that $2000\,\mathrm{km} \leqslant \Delta T \leqslant 14,000\,\mathrm{km}$ in 2050, which closely matches Figure 2(a).

7. ACCURACY OF THE ORBITS

The solution covariance is a measure of the uncertainty in the orbits, however, that uncertainty is normally optimistic

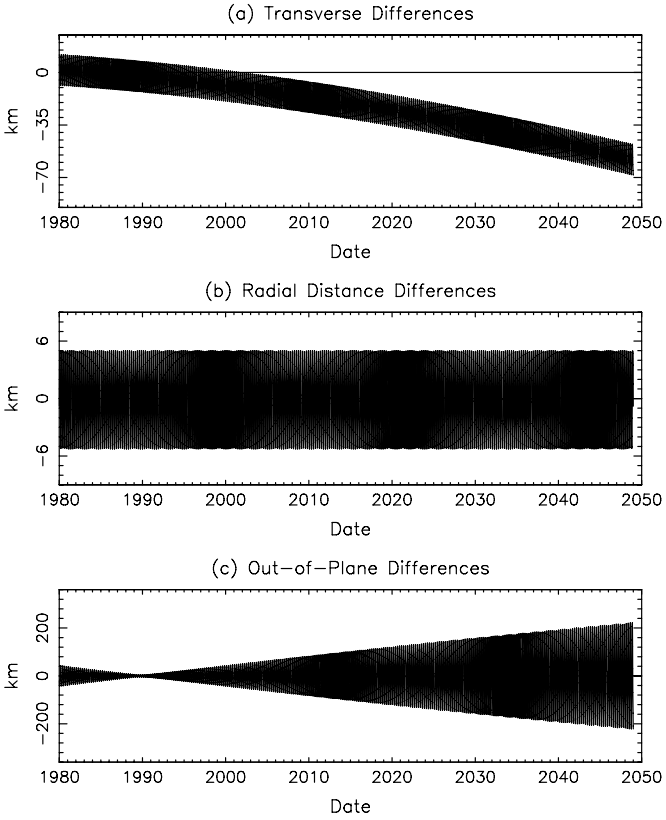

Figure 1. Triton Orbit Comparison.

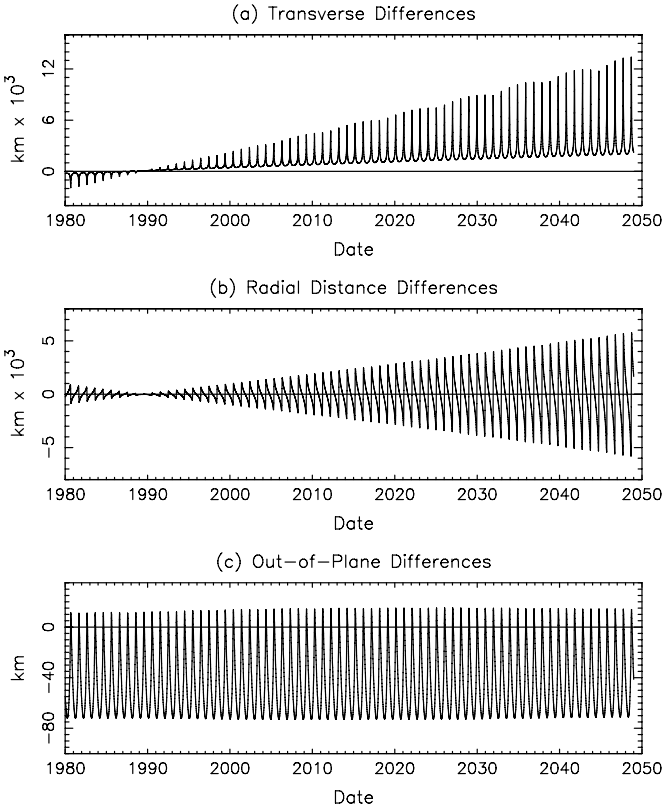

Figure 2. Nereid Orbit Comparison.

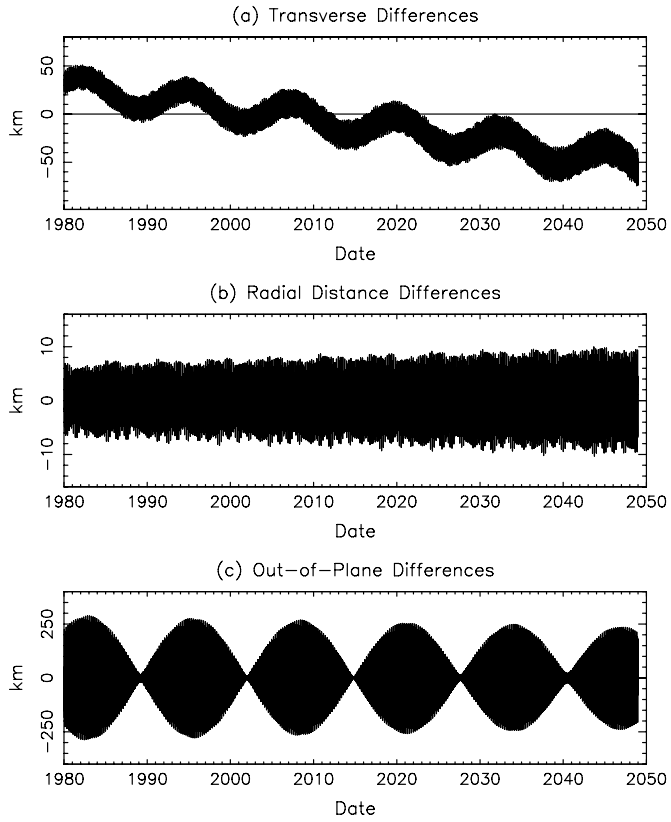

Figure 3. Proteus Orbit Comparison.

because the covariance does not account for possible systematic or unmodeled errors. Such errors can occur in the orbit or observation modeling or in the observations themselves. Because our models are quite detailed and can be fit to the observations at their presumed accuracies, we believe the dominant systematic errors are most likely in the observations.

One way to include the effect of neglected errors is to add "consider" parameters to the estimation process (Bierman 1977) to produce a "consider" covariance. The consider parameters are parameters which are not estimated but whose uncertainty contributes to the uncertainty in the estimated parameters. We considered the following.

1. Neptune's sixth zonal harmonic with an uncertainty of 0.4×10^{-6} which is 100% of the value of the harmonic based on a postulated structure for Neptune (W. B. Hubbard 2009, private communication),
2. Neptune's spin rate with the uncertainty from Table 5,
3. Neptune's moment of inertia with the uncertainty from Table 5,
4. biases in the pre-1989 relative observations with a $0\overset{\circ}{.}1$ uncertainty in position angle and $0\overset{''}{.}05$ uncertainty in separation distance,
5. biases in the post-1989 right ascension and declination astrometry with a 100 milliarcsecond (mas) uncertainty to cover instrumentation, measurement reduction, and star catalog errors,
6. biases in the post-1989 relative observations of Triton and Nereid with a 10 to 36 mas uncertainty (depending on the observer) in differential right ascension and declination,
7. biases in the Proteus *HST* observations with a $0\overset{\circ}{.}03$ uncertainty in position angle and $0\overset{''}{.}005$ uncertainty in separation distance, and
8. biases in the Proteus Earth-based astrometry with a 60 mas uncertainty.

The levels of the observation biases are based on typical observation errors. We see no evidence in our residuals of systematic errors larger than these levels.

Another way to assess the effect of neglected errors is to delete or de-weight subsets of the complete data set, refit the orbits to the altered data set, and then compare the changes in the orbits to the uncertainties derived from the consider covariance for the altered data set. If the changes are within the uncertainties, it is less likely that significant unmodeled errors are present. Consequently, the covariance can be regarded as a reasonable representation of the accuracy of the orbits. We performed an error assessment with the following altered data sets (1) the *Voyager* observations deweighted by a factor of 3, (2) all post-1989 observations removed, (3) all pre-1989 observations removed, (4) the Laborat'orio Nacional de Astrof'isca observations removed, (5) the USNO at Flagstaff observations removed, (6) the Sheshan Station and Xinglong Station observations removed, (7) the *HST* observations of Proteus removed, and (8) the Earth-based astrometric observations of Proteus removed.

In all cases the changes in the orbits were at or below the level of the uncertainties. This result suggests that we have properly accounted for all important errors and can adopt our consider covariance as our accuracy measure.

Figures 4–6 display the orbit uncertainties from the consider covariance mapped into the radial, transverse, and out-of-plane directions. As with most satellite orbits the transverse uncertainties grow due to the uncertainties in the orbital mean motion. The growth away from our integration epoch is evident. The uncertainty in Neptune's pole orientation coupled with the uncertainty in Neptune's gravitational harmonics are the primary causes of the Triton and Proteus out-of-plane uncertainties. The latter are periodic with periods equal to the orbital precession periods; the 13 year period for Proteus is obvious, the 690 year period of Triton appears as a secular growth during the 100 year time span of the figure. Nereid is unaffected by the pole and gravity harmonic errors because it is too distant to be strongly perturbed by Neptune's oblateness. Nereid's out-of-plane uncertainty is simply a consequence of its orbital inclination uncertainty. Because of its large eccentricity, Nereid's mean motion uncertainty induces the periodic in-plane uncertainties seen in Figure 5. This phenomenon is analogous to that discussed in the previous section with respect to the in-plane orbit differences. In fact, Equations (12)–(13) may be used to relate the in-plane uncertainties to the uncertainty in the mean motion.

The orbits are well determined. Even Nereid, which has the largest overall uncertainty, can be expected to be found within $0\overset{''}{.}2$ ($\approx$ 4000 km) of its predicted location for the next 100 years.

8. CONCLUDING REMARKS

This paper has reported on an update to the orbits of the Neptunian satellites. The work is essentially a repeat of that done earlier but with the addition of more astrometric observations, a change in reference frame to the ICRF, a revised Neptune pole model, a switch to a numerically integrated Proteus orbit, and an improved data processing procedure. In addition,

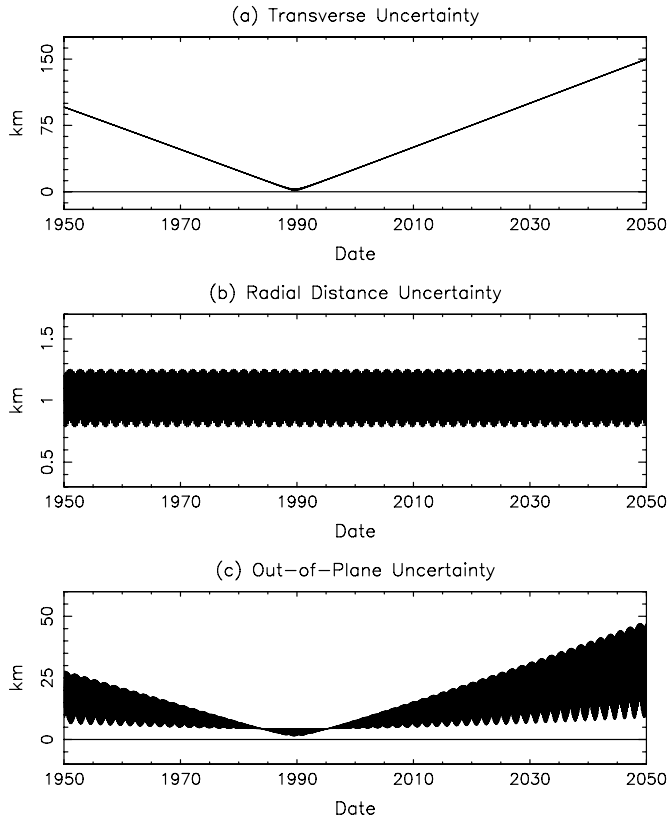

Figure 4. Triton Orbit Uncertainties.

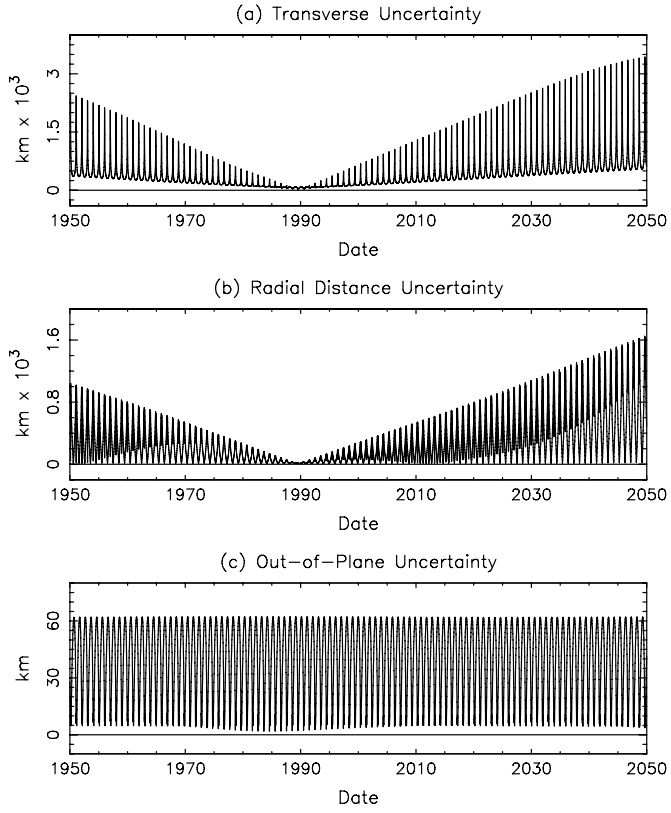

Figure 5. Nereid Orbit Uncertainties.

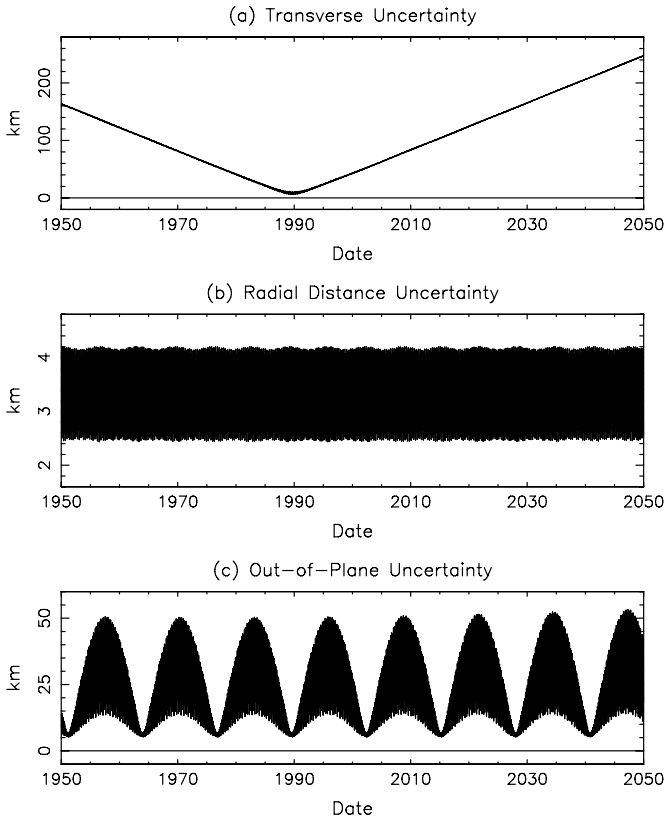

Figure 6. Proteus Orbit Uncertainties.

the *Voyager* observation modeling utilized the new *Voyager* trajectory reconstruction in the ICRF.

Ephemerides for the satellites are available electronically from the JPL Horizons online solar system data and ephemeris computation service (http://ssd.jpl.nasa.gov).

The research described in this publication was carried out at the Jet Propulsion Laboratory, California Institute of Technology, under a contract with the National Aeronautics and Space Administration.

REFERENCES

Arlot, J. E., Dourneau, G., & Le Campion, J. F. 2008, A&A, 484, 869
Bierman, G. J. 1977, Factorization Methods for Discrete Sequential Estimation (New York: Academic Press)
Colas, F., & Buil, C. 1992, A&A, 262, L13
Davies, M. E., Rogers, P. G., & Colvin, T. R. 1991, J. Geophys. Res., 96, 15,675
Dumas, C., Terrile, R. J., Smith, B. A., & Schneider, G. 2002, AJ, 123, 1776
Folkner, W. M., Williams, J. G., & Boggs, D. H. 2008, The Planetary and Lunar Ephemeris DE421, Interoffice Memo. 343R-08-003 (internal document) (Pasadena, CA: Jet Propulsion Laboratory)
Gerschultz, J. W. 1989, PHYSCON-8 Inputs Meeting, Interoffice Memo VGR-JWG-89-036 (internal document) (Pasadena, CA: Jet Propulsion Laboratory)
Hubbard, W. B., Podolak, M., & Stevenson, D. J. 1995, in Neptune and Triton, ed. D. P. Cruikshank (Tucson, AZ: Univ. Arizona Press), 109
IAU 2006, in Resolution B3: Re-Definition of Barycentric Dynamical Time, TDB, International Astronomical Union, Paris, France, http://www.iau.org
Jacobson, R. A. 1990, A&A, 231, 241
Jacobson, R. A. 1991, A&AS, 90, 541
Jacobson, R. A. 2008, Reconstruction of the *Voyager* 2 Neptune Encounter in the ICRF System, AIAA Paper 2008-7372 Presented at the AIAA/AAS Astrodynamics Specialist Conference, Honolulu, HI (Reston, VA: American Institute of Aeronautics and Astronautics)
Jacobson, R. A., & Owen, W. M., Jr. 2004, AJ, 128, 1412
Jacobson, R. A., Riedel, J. E., & Taylor, A. H. 1991, A&A, 247, 565

Lewis, G. D., Taylor, A. H., Jacobson, R. A., Roth, D. C., Riedel, J. E., Synnott, S. P., & Ryne, M. S. 1992, J. Astronaut. Sci., 40, 369
Marchis, F., Urata, R., de Pater, I., Gibbard, S., Hammel, H. B., & Berthier, J. 2004, BAAS, 36, 860
Martins, R. V., et al. 2004, A&A, 425, 1107
MPC 2000, Circular No. 38967, 40914, Minor Planet Center, Smithsonian Astrophysical Observatory, Cambridge, MA
MPC 2001, Circular No. 43261, 44182, Minor Planet Center, Smithsonian Astrophysical Observatory, Cambridge, MA
MPC 2002, Circular No. 46216, 46508, Minor Planet Center, Smithsonian Astrophysical Observatory, Cambridge, MA
MPC 2003, Circular No. 49424, Minor Planet Center, Smithsonian Astrophysical Observatory, Cambridge, MA
MPC 2004, Circular No. 52492, 52493, 52765, 52887, 53171, Minor Planet Center, Smithsonian Astrophysical Observatory, Cambridge, MA
MPC 2005, Circular No. 54343, 54557, 54698, 54823, 54965, 55508, Minor Planet Center, Smithsonian Astrophysical Observatory, Cambridge, MA
MPC 2006, Circular No. 56794, 57110, 57416, 57417, 57573, 57574, 57792, 57793, 57947, 58097, Minor Planet Center, Smithsonian Astrophysical Observatory, Cambridge, MA
MPC 2007, Circular No. 59029, 59581, 59860, 60086, 60268, 60451, 60647, 60906, 61163, Minor Planet Center, Smithsonian Astrophysical Observatory, Cambridge, MA
MPC 2008, Circular No. 62864, 63123, 63363, 63584, 63806, 64093, Minor Planet Center, Smithsonian Astrophysical Observatory, Cambridge, MA
Owen, W. M. J., Vaughan, R. M., & Synnott, S. P. 1991, AJ, 101, 1511
Pascu, D., et al. 1999, BAAS, 31, 1229
Peters, C. F. 1981, A&A, 104, 37
Qiao, R. C., Cheng, X., Shen, K. X., Dourneau, G., Wang, S. H., Hu, X. Y., Tang, Z. H., & Xi, X. J. 2008, MNRAS, 391, 1791
Qiao, R. C., et al. 2007, MNRAS, 376, 1707
Seidelmann, P. K., et al. 2007, Celest. Mech., 98, 155
Stone, R. C. 2000, AJ, 120, 2124
Stone, R. C. 2001, AJ, 122, 2723
Stone, R. C., & Harris, F. H. 2000, AJ, 119, 1985
Tapley, B. D., Schutz, B. E., & Born, G. H. 2004, Statistical Orbit Determination (Burlington, MA: Elsevier)
Van Biesbroeck, G. 1951, AJ, 56, 110
Van Biesbroeck, G. 1957, AJ, 62, 272
Van Biesbroeck, G., Vesely, C. D., Aksnes, K., & Marsden, B. G. 1976, AJ, 81, 122
Veiga, C. H., & Vieira Martins, R. 1996, A&AS, 120, 107
Veiga, C. H., & Vieira Martins, R. 1998, A&AS, 131, 291
Veiga, C. H., Vieira Martins, R., & Le Guyader, C. 1999, A&AS, 136, 445
Veiga, C. H., Vieira Martins, R., Le Guyader, C., & Assafin, M. 1996, A&AS, 115, 319
Warwick, J. W., et al. 1989, Science, 246, 1498
Zharkov, V. N., & Trubitsyn, V. P. 1978, in Physics of Planetary Interiors, trans. W. B. Hubbard (Tucson, AZ: Pachart Press)